ELSEVIER

Contents lists available at ScienceDirect

Acta Materialia

journal homepage: www.elsevier.com/locate/actamat





Mapping high entropy state spaces for novel material discovery

Johnathan von der Heyde^a, Walter Malone^{b,*}, Abdelkader Kara^{a,c}

- ^a Department of Physics, University of Central Florida, Orlando, FL, 32816, USA
- ^b Department of Physics, Tuskegee University, Tuskegee, AL, 36088, USA
- ^c Applied Chemistry and Engineering Research Centre of Excellence, Mohammed VI Polytechnic University, Ben Guerir, 43150, Morocco

ARTICLE INFO

Keywords: High entropy Machine learning Density functional theory

ABSTRACT

High-entropy alloys show promising properties for novel catalytic designs, but their vast potential configurations make them challenging to study computationally. Additionally, the traditional methods for data acquisition required to train neural networks on these broad systems can be inefficient. To address this, we propose an active learning methodology that integrates genetic algorithms with deep convolutional neural networks trained on Density Functional Theory calculations via a simple closed feedback loop. This approach streamlines data acquisition and the exploration of large configurational spaces simultaneously. We illustrate its effectiveness on high-entropy clusters of variable sizes and compositions, the vast state spaces of which are automatically explored and trained on, so as to generate and predict the stability of any cluster within the latent space given minimal computational requirements. Importantly, this method is adaptable for use in a variety of other systems of different sizes, chemical compositions, and stoichiometry.

1. Introduction

High-entropy alloys (HEAs), alloys with generally five or more elements, are a novel class of materials involving many principal elements. They offer a broad range of applications beyond low entropy alloys (LEAs) by combining unique properties like strength, ductility, corrosion resistance, thermal stability, among others [1–3], as well as fine-tuned catalytic behavior [4–6], all in one material. However, these unique properties derive from specific elemental compositions, stoichiometries, and geometries, and so are not easily predicted *a priori* due to the vast space of complex, combinatoric possibilities. Therefore, many have turned to machine learning (ML) methods to learn chemical patterns in experimental and theoretical data and hence infer predictive design with significant accuracy [7–18]. Studies exist, for example, that predict the ductility [10], hardness [8,14,18], surface energies [13], as well as other properties of HEAs [15–17].

The bottleneck for these data-driven predictive models is of course data acquisition. Due to the immense scale of the combinatoric space available to HEAs, no reasonable method exists for exploring these possibilities thoroughly. Only very recently have more advanced techniques been applied together with neural networks (NNs) and other ML methods in order to further improve efficiency [19–26]. To this end, our work addresses this bottleneck and expands upon the research from a

theoretical standpoint by demonstrating how one can engineer a feed-back loop between structures generated and structures validated within an active learning algorithm (ALA).

ALAs have been used successfully in material discovery for exploring vast search spaces of promising potential without the need for human-inthe-loop verification [27-41]. Notable examples include ALA techniques utilized to optimize for wide band-gap materials [39], surface reaction networks [40], and melting temperatures [41]. Many ALAs that seek to explore chemical space utilize what is known as query-by-committee, where one builds an ensemble of models and focuses training on areas of the phase space with large, normalized ensemble standard deviation. For high entropy materials, other approaches have also gained traction [42-50]. Notable examples include a study where Rao et al. employed a complex active learning loop between experiment and theory to study high-entropy materials. They began with an autoencoder and stochastic sampling technique for generating and sampling structures. Then with a two-step ensemble regression model and a gradient-boosting decision tree they narrowed down promising high entropy materials. A ranking policy selected the final candidates, which were experimentally validated [46]. Xue et al., looking to find high entropy alloys with low thermal hysteresis, found success using a Bayesian-based approach with bootstrap sampling to estimate uncertainty and guide where to supplement their dataset of first-principles calculations [47]. Li et al. employed

E-mail address: wmalone@tuskegee.edu (W. Malone).

https://doi.org/10.1016/j.actamat.2024.120237

^{*} Corresponding author.

a domain knowledge constrained active learning loop with Bayesian optimization and bootstrap sampling to search for high-entropy alloys by ultimate strength and ductility [48]. Sulley also utilized a Bayesian optimization approach to predict the stable phases of high-entropy alloys [49]. Zhang et el., like the previous study, focused on predicting the phases of high-entropy alloys, but instead used a genetic algorithm to pick specific ML models and descriptors [50]. Our ALA methodology is similar in design to previous methodologies, wherein a closed feedback loop is established between structures sampled, and structures used to improve an inference model, which in-turn improves the decision making algorithm for prioritizing the sampling of novel data - a broad view of implementations and their applications can be found in literature reviews [28,38]. Here we present a simple approach that scans phase space for lower atomization energies, simultaneously building up our training dataset while proceeding closer to an energy minimum. Our approach also reduces the number of high-entropy data points needed to train models to predict the properties of high entropy materials by making use of low-entropy, bimetallic data.

In a previous report [51] we established the ALA's functionality with bimetallic nanoclusters of various sizes, where it was discovered that training on exclusively 15, 20, and 25 atom clusters allowed us to successfully interpolate and infer the energies and forces of clusters between these sizes with high accuracy, ~0.3 eV mean absolute error (MAE) in all energy predictions. This proved the NN was learning the energy landscape as a function of cluster configuration with minimal bias, allowing us to dramatically reduce the compute naively required for generalization by training specifically on uniquely representative clusters. Now, we expand the ALA's domain of applicability by testing it on high-entropy clusters (HECs) of various sizes, stoichiometries, and compositions.

As proof-of-concept, we focus on HECs, rather than bulk or substrate alloys, because they have advantages in their high surface-to-volume ratio, allowing for wider ranges in coordination and hence reactivity, which is essential for novel catalytic design [52-55]. The ALA combines a genetic algorithm (GA) for generating structures and density functional theory (DFT) for validating or 'labeling' said structures. GAs have a long history of use in exploring the conformational space of metallic clusters [55-65,18], with most attempts however involving only low-entropy systems. In this work, we explore the chemical space of six elements: Ag, Au, Cu, Ni, Pd, and Pt, and show that one can reliably predict HEC energies (~0.3 eV MAE across all tests) and forces at the quantum level in a highly efficient and automatic way. Taken together, our results demonstrate the ability to generalize from low-to-high entropy clusters, as well as between small and large clusters. Specifically, we show how the ALA trained to predict energies and forces for bimetallic clusters of sizes 33, 55, and 77 atoms can reliably predict the energies and forces of clusters with up to six elements, as well as successfully interpolate predictions for clusters between these sizes. By relying on bimetallic data and only three cluster sizes, we can save vast amounts of computational resources exploring HECs.

Stoichiometries per cluster size are generated randomly from their binomial distributions such that they maintain mostly even elemental and stoichiometric ratios. If one instead uses a NN to train an interatomic potential for a specific stoichiometry or range of stoichiometries, as has become popular [22-26], there is no guarantee, and indeed it is unlikely, that this potential performs well on different stoichiometries, severely limiting the high-entropy chemical space that we can reliably explore. And so by generating cluster compositions from their total possibilities in a random yet controlled fashion, maintaining uniform elemental and stoichiometric distributions, we minimize bias across these combinatoric possibilities. Counting the total number of allowed stoichiometries S is relatively straightforward with combinatorics: let zbe the set of available elements $z = \{Ag, Au, Cu, Ni, Pd, Pt\}, c$ the choice in number of elements per cluster, measuring the entropy of our system, $c = \{2, 3, 4, 5, 6\}$, and n the size of the system. The total number of possible stoichiometric combinations can therefore be

counted

$$S = \begin{pmatrix} z \\ c \end{pmatrix} \begin{pmatrix} n-1 \\ c-1 \end{pmatrix} \tag{1}$$

The first factor is understood to be the number of ways one can choose c elements from z options, and the second factor is derived directly from the 'stars and bars' theorem for combinations with repetition. Total combinations S grows quickly in all of its parameters. For example, if we have 55-atom clusters of six total possible elements per cluster, we have $S=8.10\times10^2,\ 2.86\times10^4,\ 3.72\times10^5,\ 1.9\times10^6,\ 3.16\times10^6$ stoichiometries for $c=2,\ 3,\ 4,\ 5,\ 6$ respectively. Note that this says nothing about geometry, we are simply counting all possible unique combinations of elements and elemental ratios. Thus, if we had a larger system of 100 atoms and 10 elements to choose from, we already have approximately a trillion possible stoichiometric combinations for any given geometric configuration. This expression of the vastness of the state space is the underlying motivation for merging sophisticated search algorithms and machine learning techniques.

Our results suggest fully automatic data generation and validation for mapping these vast state spaces at high accuracy, in identifying both global patterns and unique local states, is very much possible with reasonable computational demands. The overall compute saved by combining sophisticated search algorithms with machine learning techniques, as compared to traditional methods, cannot be overstated. In Section 2 we present our computational methods, in Section 3 we present our results & discussion, and in Section 4 we present our conclusions.

2. Computational methods

Active learning is an ML technique that typically involves feedback loops for self-optimization and allows the algorithm to actively decide what data to use as it iterates, e.g., which data to label for training a NN. The ALA's algorithm and schema are simplified in Fig. 1, where one global iteration is defined by the outermost "for loop". Here, this decision-making is achieved by the filtration functions F1 and F2. The first filtration function decides which of the images generated by the GA to label via DFT. The second filtration function likewise decides which of the labeled images to use for training the NN. Together, they can be optimized to minimize costly DFT calculations and train exclusively on minimally necessary images. In our example, F1 primarily ensures clusters are 'safe', in that they obey interatomic distances and cell constraints with a minimal interatomic distance of 0.2 Å and cell bounds of 20 Å, with the additional function of maintaining size and stoichiometric distributions within the dataset. F2 likewise filters out any mislabels, maintains distributions, and can use the previous iteration's NN to infer which images to select, minimizing training redundancy and ensuring diversity within the training dataset per global iteration.

The GA is implemented via the Atomic Simulations Environment

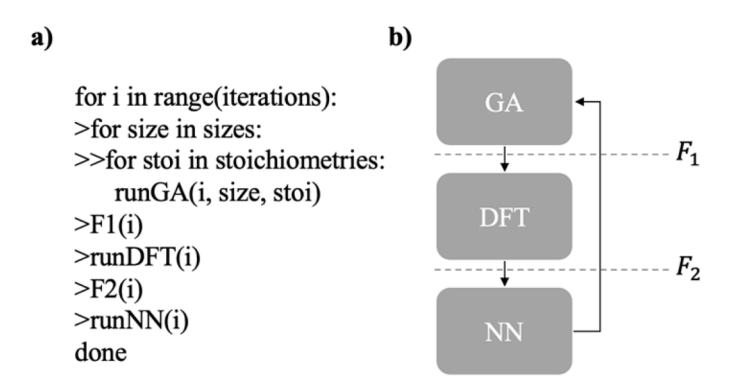


Fig. 1. ALA simplified algorithm (a), and schema (b). Global iterations are defined by the outer "for loop".

(ASE) library [66]. It works by taking in system constraints and generating an initial population of images, and then a process of 'evolution' occurs. Images are selected based on a 'fitness function', possible 'mutations' occur, and pairs are combined via 'crossover' functions, generating new structures. This process of selection, mutation, and crossover constitutes one generational cycle and can be iterated to 'evolve' novel and evermore fit images (structures). In our demonstration, the fitness function is simply the cluster's atomization or binding energy, defined as the difference in its total energy (TE) and the sum of energies E_i of its constituent atoms

$$AE = TE - \sum E_i \tag{2}$$

Thus, our GA performs a global optimization search on cluster atomization energy as a function of configuration. We chose to allow our GA algorithm to modify cluster geometry and stoichiometry with respect to atomization energy as we are interested in screening for clusters that may be experimentally synthesized. While atomization energy may not be a perfect indicator of which clusters may form under experimental conditions, it serves as a useful metric for reducing state space, allowing us to screen a much smaller subspace of clusters with high-level theoretical calculations or with experiment. Moreover, if our algorithm works with atomization energy as a fitness function, it should work with any other calculatable quantity. Evolutionary algorithms are in general well-known to be efficient and unbiased search techniques due to their ability to balance exploration and exploitation via their tunable parameters and inherent stochastics. We start with 100 initial random images and generate from them 500 images per size, per stoichiometry, per global iteration. We use a mutation rate of 0.3, for mirror, rattle, and permutation mutations as implemented by ASE. Each set of 500 images is then filtered down by F1 to the top 50 images sampled from a lognormal distribution over their atomization energies. This leads to just 500 images per cluster size, per global iteration, for labeling with DFT.

The DFT validation labeling is implemented via the VASP package 5.4 [67–69], which we use to calculate a given image's total energy and forces. These simulations are externalized from Python, such that they may be more easily parallelized on a large compute cluster. We use the GGA functional from PBE [70] with the PAW [71] method, a $1\times1\times1$ k-point mesh, 50–100 electronic iterations, under a minimal energy difference of 1E-4 eV, and no positional update. F2 then filters these images, if need be, ensuring they converge to reasonable energy and force values. Moreover, F2 can ensure no new images are energetically redundant within the training set, maintaining efficiency and diversity.

The NN is implemented via the SchNetPack library [72], which uses a deep convolutional approach for modeling atomistic properties such as potential energy surfaces and other quantum-chemical properties of

molecules and materials. For our purposes, we use it to learn the pairwise DFT potentials, so as to predict cluster energies and forces from geometry and composition around 1000x faster than DFT, with reliable precision and accuracy. We train each global iteration's cumulative dataset for 500 epochs, or until no improvements to the validation loss occur over 50 epochs, with a starting learning rate of 0.001, which reduces by half every 20 epochs that don't improve by a relative change of 0.1 %. We use a 70, 15, and 15 percentage split for training, validation, and testing datasets, respectively.

To demonstrate the efficiency of our methodology, we first run the ALA to convergence, given our criteria, with all possible types of bimetallic clusters, given our six elements of sizes 33, 55, and 77 atoms. Then we test how well the final NN interpolates the energies and forces of clusters between the range of 33 and 77 atoms and between low and high entropy, from two up to six elements.

3. Results & discussion

Global convergence is seen in Fig. 2a and b, where after 8 global iterations, we determine our cumulative NN to have successfully learned the DFT potential for the given state space of bimetallic 33, 55, and 77 atom clusters. Here the ALA is considered to converge when the MAEs fail to improve significantly between successive iterations. We notice that the global improvement is not monotonic, as iterations can fare worse than previous iterations. This behavior is expected since, while the state space is simplifying globally, due to the fact that generated clusters are becoming more relaxed and symmetric via the GA's implementation, it is not always simplifying locally. For instance, we often have an up-tick in MAEs when the clusters transition from an open, random distribution, to a closed, more orderly configuration – not unlike how relaxation curves often involve potential barriers that need to be overcome before deeper minima are achieved, the same principle applies to the global state space. The fact is, we could use our filtration functions, F1 and F2, to emphasize structures the NN knows well, and we would get a more monotonic trajectory, at the cost of over-specializing the NN, and so a balance must be struck between training on novel and familiar images.

Once our ALA has converged, we put the cumulative NN to the test of generalization (explicit training results are seen in the supplementary material Fig. S1). Fig. 2c shows these results for the NN trained exclusively on LECs (bimetallic clusters) again for 33, 55, and 77 atom clusters, where the NN is attempting to generalize from LECs to HECs, and performs surprisingly well. Each set of energies and forces per entropy, per graph, contains approximately 500 images generated by a GA and validated with DFT, external to the ALA. We see a more or less constant

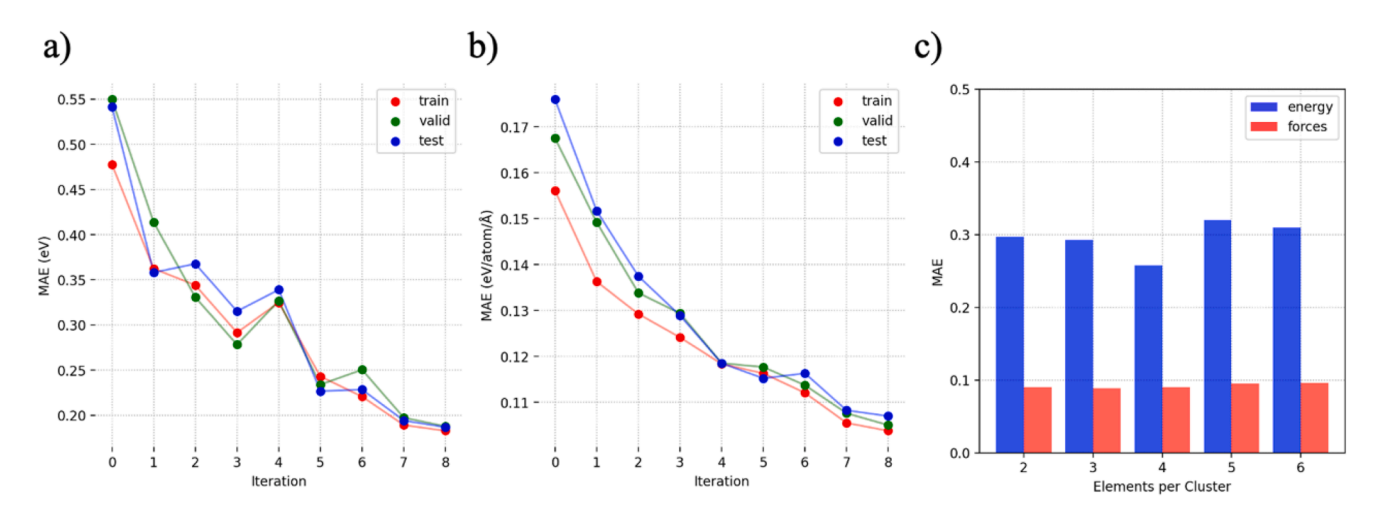


Fig. 2. Mean absolute error (MAE) on prediction for energies (eV/cluster) in a), and forces (eV/atom/Å) in b), show learning improvement as a function of global iteration. Low-to-high entropy predictions in the same units c). Datasets were trained exclusively on bimetallic clusters of sizes 33, 55, and 77 atoms.

MAE as a function of entropy. This result is what one would expect if the NN was approximating the DFT potential well, as there should be minimal bias concerning system entropy, and importantly, this indicates we can predict high-entropy systems from low entropy ones, without the computational increase that is typically associated with increased system complexity.

Now that we have evidence for the algorithm's ability to use LECs to predict HECs, we want to test size interpolation and entropy extrapolation simultaneously. Since in our previous report we have shown that these NNs can successfully predict between and around cluster sizes used for training, we now want to see if they can do the same for high entropy systems, and to what extent. This test is a direct measure of the extent to which the NN has learned the DFT potential – because if it has learned the potential well, then just like DFT, its accuracy should not be affected by the size of the system or combinations of its constituent atoms. Of course some deviation is expected, since the NN is only approximating the DFT potential, given the trained dataset, and making extrapolations. However, the point of using NNs like this is precisely to trade in some affordable error to obtain a very reasonable prediction several orders of magnitude faster than the associated first-principle calculation.

Fig. 3 shows these results. The first graph shows rolling averages of the energy MAEs of each subsequent graph collectively. Whereas in Fig. 2c), every adjacent blue-red bar pair represents approximately 500 test clusters of the graph's associated size(s), per entropy, here they represent ~100 test clusters of the graph's associated entropy, per size. That is, here in Fig. 3, the x-axis spans all cluster sizes between 33 and 77 atoms inclusively, and for each size we plot an associated MAE for the

energy and forces over $\sim \! 100$ clusters of that size. The rolling average of the first graph's window is every 5 cluster sizes, and so each point in the associated entropy's colored line is composed of an average of the energy MAE for $\sim \! 500$ test clusters, again generated by a GA, and validated with DFT, external to the ALA – force MAEs are ignored in the first plot to ease visualization of the energy error distribution.

The general trends here are obvious, firstly the NN seems to present robustness regarding the given cluster's entropy. Additionally, by training on exclusively 33, 55, and 77 atom clusters, the NN can infer with scattered but predictable accuracy for all sizes in between, meaning the NN can predict with a MAE for atomization energy of less than 0.40 eV and a MAE for forces below 0.25 eV/Å for most cluster sizes in between 33, 55, and 77 atoms. The first two trends are taken to be evidence for the NN approximating the DFT functional well. Some outliers with larger MAEs exist. We see these outliers generally at lower cluster sizes. That is to say, the NN prediction error is somewhat inversely proportional to cluster size. This last trend, the downward slope of MAE vs cluster size, can be understood by realizing smaller clusters have less diversity within their coordination trends, whereas larger clusters can encapsulate the coordination trends of smaller clusters into their own. That is to say, geometric and elemental patterns made by smaller clusters can be picked up on by the NN from pieces of larger clusters, whereas the reverse is not true. As the NN predicts with less accuracy on smaller clusters, we also expect the error per atom to be larger for the smaller clusters and smaller for the larger clusters. This exact trend is demonstrated in Figure S2 in the Supplementary information. Figure S2 contains the same plots as Fig. 3 but with errors in eV/atom. Finally, we do not see noticeable outliers for force predictions on clusters with sizes

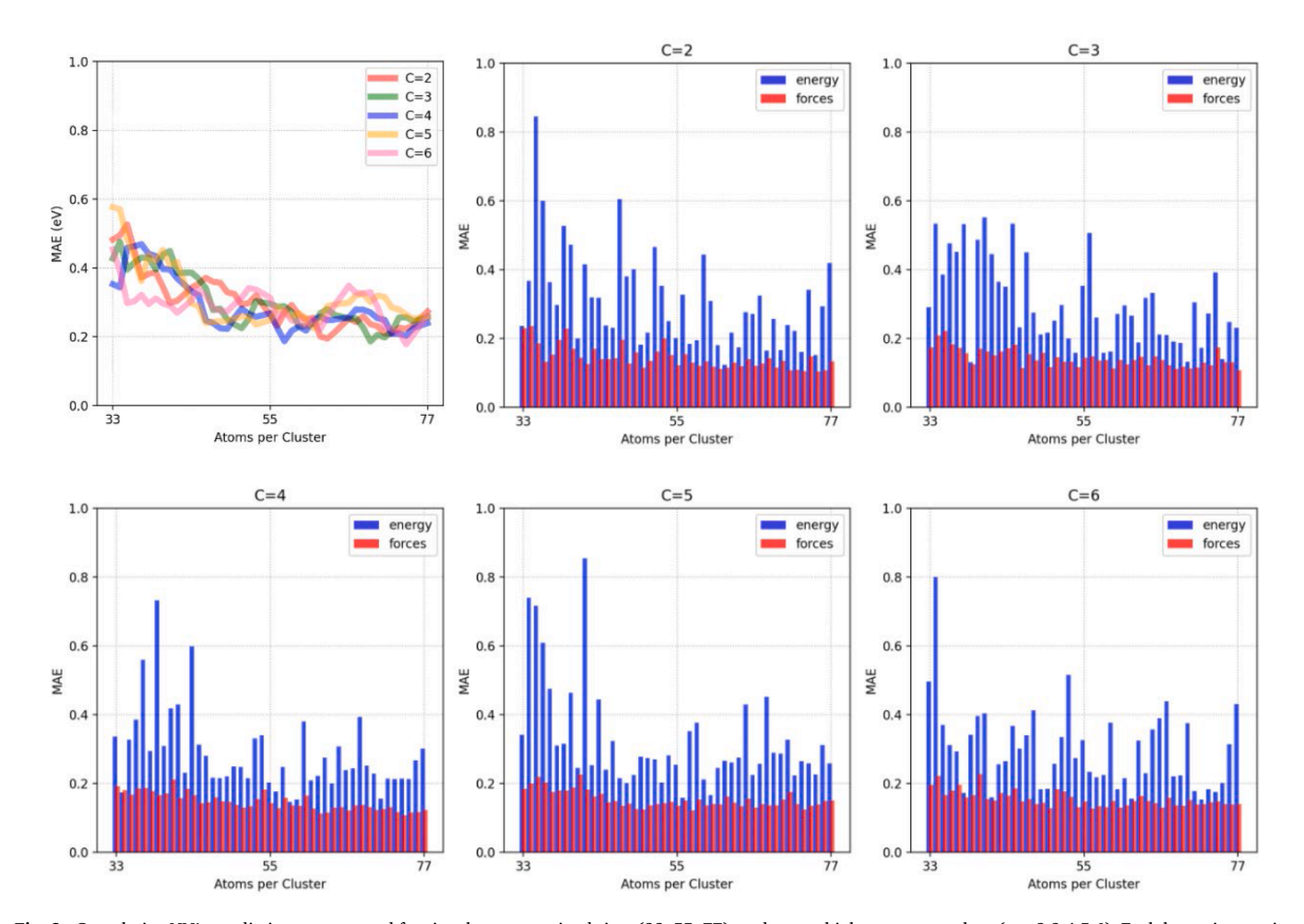


Fig. 3. Cumulative NN's prediction errors tested for sizes between trained sizes (33, 55, 77), and across higher entropy values (c = 2,3,4,5,6). Each bar pair contains ~100 test images generated external to the ALA of random, even stoichiometry. Units are again eV for energies and eV/Å for forces.

outside the training dataset. We attribute this to the fact that our algorithm is converging on some local or global energy minimum, where the forces on each atom will all be close to zero.

Focusing on the bimetallic clusters the algorithm trains on, during the ALA's descent toward the system's global minima, the configuration space is mapped as a function of energy. That is, the set of clusters generated, sampled, and labeled during this process automatically represent some estimation of the otherwise intractable state space topology. Therefore, we can infer unique states and global patterns from this collection and its statistical distributions. As exemplified in Fig. 4, we showcase the highest and lowest unique structures with respect to both their total energy and atomization energy as the ALA explores bimetallic clusters. A few noteworthy trends stand out. Firstly, Pt clusters dominate the most stable states, be they in terms of total or atomization energy, with few exceptions - note that no pure clusters exist in the datasets, they are all composed of at least two elements. Additionally, the least stable total energy structures are populated mostly by Ag-Au clusters, with a few Ag-Pd and Ag-Cu as well, whereas in terms of atomization energy, we see many more Pd clusters, not all of which contain Ag. These differences stand to justify the importance of calculating atomization or binding energy as a more representational measure of structure stability, as compared to total energy. We see the use of this more relative measure in the fact that the most stable structures are more consistent, as well as the fact that the least stable structures are more diverse. We also note more disorder among clusters with the highest atomization energy, which should be expected. As our ALA moves towards an atomization energy minimum, the clusters adopt a much more ordered phase.

To get a better understanding of this energy landscape, we plot several distributions in Fig. 5, which stand to demonstrate what global patterns can be gleaned from our ALA methodology. We sample 9000 images of those generated and validated and plot their atomization energies as a function of cluster size (black lines in the first plot). We see that they span a wide overlapping range of -40 to -375 eV, and by plotting which element is most common for each cluster (here as

different colors), we can get an idea of the stability contributions per element. Fig. 5b) emphasizes this relation by normalizing the distribution of each cluster's stability as a function of its most common element (same colors). Clearly, Pt and Ni dominate the most stable clusters regardless of size, and Ag and Au compose most of the least stable structures. Moreover, we can compare these elemental and energetic distributions directly with core-shell segregation - that is, how the elements prefer to gather within the cluster, as either in the core, on the surface, or some other mixed morphology. This shows which elements will be more or less susceptible to reaction conditions. For example, we note that while Pt and Ni dominate the most stable clusters, Pt doesn't prefer the core, rather, Ni and Cu do, while Au and Ag prefer the surface, where the rest are mixed. These insights into global and local patterns come automatically and without bias from the ALA's data generation and validation methodology, providing us with meaningful trends of significant interest to the new era of materials discovery.

4. Conclusions

We have demonstrated the utility of a new ALA design, in its ability to self-improve as it descends the energy landscape, generating, sampling, and labeling new images to learn from. This procedure serves specifically for exploring vast new state spaces, for which no data is readily available, and will by design converge automatically on or around the state space's global energy minima complete with a cumulative neural network capable of accurately predicting the energies and forces (and perhaps other properties) of any reasonable structure (defined by filtration functions) within the system's state space. Moreover, we have provided evidence for the fact that low-entropy systems' characteristics can indeed be used to predict the formation of highentropy systems. Specifically, we demonstrated that the ALA trained on bimetallic clusters can successfully make predictions on clusters with up to six elements, and between all trained sizes. All energy prediction MAEs are less than 1.0 eV per cluster, and decrease towards ~0.2 eV with increasing cluster size scale. The cluster's total energy ranges

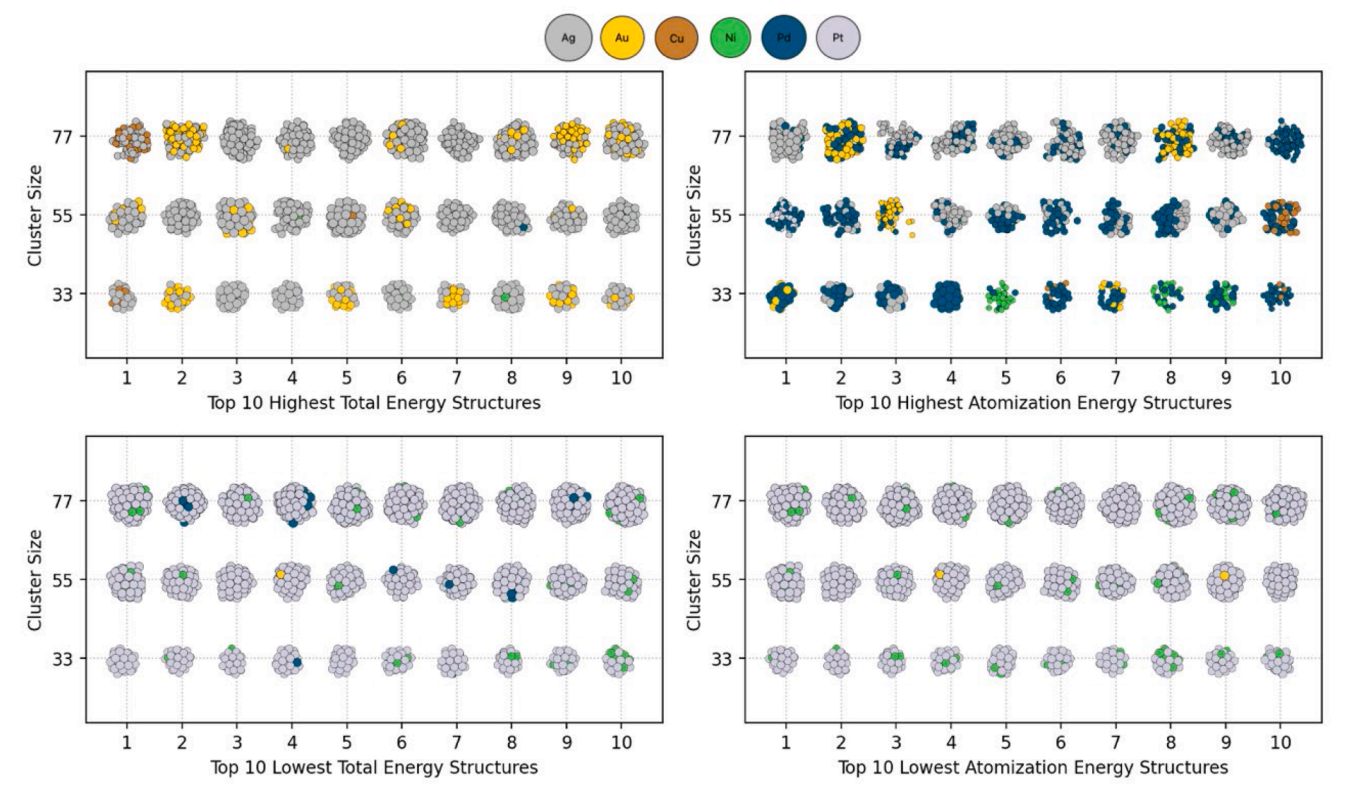


Fig. 4. Generated and validated bimetallic clusters showcasing geometric, compositional, and stoichiometric preferences.

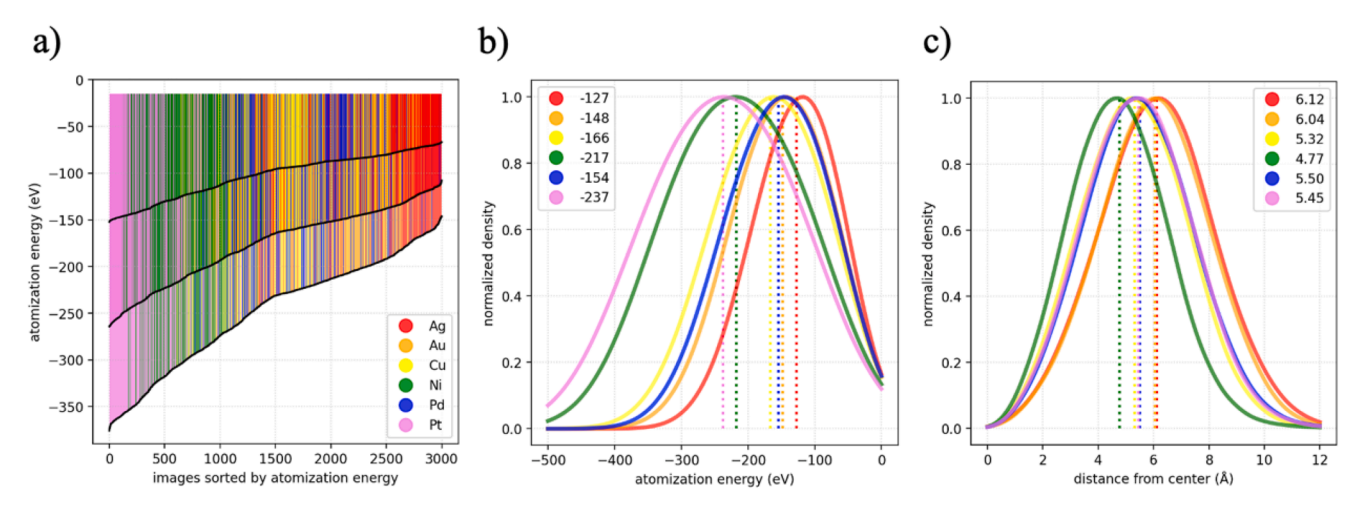


Fig. 5. 3000 images sampled randomly across energy distributions for each cluster size (33, 55, 77). Atomization energy plots a) with the corresponding image's most common element as vertical bars, and b) with all image's most common element as distributed as a gaussian. Distance from cluster's geometric center c) as a function of all image's most common element, again distributed as a gaussian (with kernel density estimation using Scott's factor for covariance).

between -50 and -400 eV, and therefore, assuming an average MAE of 0.3 eV, our energy errors range from 0.075 % to 0.6 % of the total energy – with force errors consistently smaller. We thereby demonstrate that a properly trained NN can generalize from LECs to HECs and interpolate to cluster sizes never seen before. While these results come naturally with the assumption that our neural networks have accurately modeled the DFT potential, which can itself generalize, they nevertheless represent extremely valuable insights for dramatically reducing the computational cost of simulating complex systems, as is inherent in the search for novel high entropy materials. Moreover, since our algorithm works well minimizing atomization energy, it should work well for other properties of HECs. Future studies will focus on the ability of our method to other properties, and to size extrapolation.

The importance of this computational frugality cannot be overstated, for simulating high-entropy systems via DFT involves notably larger compute compared to low-entropy systems of the same design, due to greater electronic complexity. Yet, a NN which has approximated the DFT potential will predict system properties in constant runtime regardless of system complexity. This allows us to make quantumaccurate guesses for complex systems from low-complexity data, effectively circumventing the exponential compute typically associated with the scaling of non-linear systems. To conclude, we believe the methodology presented in this study represents a significant step forward in the computational exploration of high-entropy systems, demonstrating the potential of active learning, and machine learning methods in general, in tackling complex materials science problems. The development and successful implementation of our ALA paves the way for future studies to further harness and exploit the unique properties of high-entropy materials for practical applications, especially in the field of catalysis and hydrogen storage. This basic algorithmic feedback design could very well be instrumental in guiding experimental efforts by providing insights into promising configurations and phases for complex materials.

CRediT authorship contribution statement

Johnathan von der Heyde: Writing – review & editing, Writing – original draft, Visualization, Validation, Methodology, Investigation, Formal analysis, Data curation. Walter Malone: Writing – review & editing, Supervision, Methodology, Conceptualization. Abdelkader Kara: Writing – review & editing, Supervision, Methodology, Conceptualization.

Declaration of competing interest

The authors declare that they have no known competing financial interests or personal relationships that could have appeared to influence the work reported in this paper.

Acknowledgements

Walter Malone acknowledges support from the National Science Foundation RISE grant # 2122985.

Supplementary materials

Supplementary material associated with this article can be found, in the online version, at doi:10.1016/j.actamat.2024.120237.

References

- [1] Y. Zhang, T. Zuo, Z. Tang, M. Gao, K. Dahmen, P. Liaw, Z. Lu, Microstructures and properties of high-entropy alloys, Prog. Mater. Sci. 61 (2014) 1–93.
- [2] Y. Ye, Q. Wang, J. Lu, C. Liu, Y. Yang, High-entropy alloy: challenges and prospects, Mater. Today 19 (2016) 349–362.
- [3] W. Zhang, P. Liaw, Y. Zhang, Science and technology in high-entropy alloys, Sci. China Mater. 61 (2018) 2–22.
- [4] T. Batchelor, J. Pedersen, S. Winther, I. Castelli, K. Jacobsen, J. Rossmeisl, Highentropy alloys as a discovery platform for electrocatalysis, Joule 3 (2019) 834–845.
- [5] Y. Sun, S. Dai, High-entropy materials for catalysis: a new frontier, Sci. Adv. 7 (2021).
- [6] H. Li, J. Lai, Z. Li, L. Wang, Multi-sites electrocatalysis in high-entropy alloys, Adv. Funct. Mater. (2021) 31.
- [7] W. Huang, P. Martín, H. Zhuang, Machine-learning phase prediction of highentropy alloys, Acta Mater. 169 (2019) 225–236.
- [8] C. Wen, Y. Zhang, C. Wang, D. Xue, Y. Bai, S. Antonov, L. Dai, T. Lookman, Y. Su, Machine learning assisted design of high entropy alloys with desired property, Acta Mater. 170 (2019) 109–117.
- [9] Z. Rao, P. Tung, R. Xie, Y. Wei, H. Zhang, A. Ferrari, T. Klaver, F. Körmann, P. Sukumar, A. Silva, Y. Chen, Z. Li, D. Ponge, J. Neugebauer, O. Gutfleisch, S. Bauer, D. Raabe, Machine learning-enabled high-entropy alloy discovery, Science 378 (2022) 78–85.
- [10] X. Huang, L. Zheng, H. Xu, H. Fu, Predicting and understanding the ductility of BCC high entropy alloys via knowledge-integrated machine learning, Mater. Des. 239 (2024) 112797.
- [11] K. Kaufmann, K.S. Vecchio, Searching for high entropy alloys: a machine learning approach, Acta Mater. 198 (2020) 178–222.
- [12] Z. Zhou, Y. Zhou, Q. He, Z. Ding, F. Li, Y. Yang, Machine learning guided appraisal and exploration of phase design for high entropy alloys, Npj Comput. Mater. 5 (2019) 128.
- [13] Y.-J. Hu, A. Sundar, S. Ogata, L. Qi, Screening of generalized stacking fault energies, surface energies and intrinsic ductile potency of refractory multicomponent alloys, Acta Mater. 210 (2021) 116800.

[14] X. Huang, C. Jin, C. Zhang, H. Zhang, H. Fu, Machine learning assisted modelling and design of solid solution hardened high entropy alloys, Mater. Des. 211 (2021) 110127

- [15] Y. Zhou, P. Srinivasan, F. Körmann, B. Grabowski, R. Smith, P. Goddard, I.A. Duff, Thermodynamics up to the melting point in a TaVCrW high entropy alloy: systematic ab initio study aided by machine learning potentials, Phys. Rev. B 105 (2022) 214302.
- [16] Z. Fan, B. Xing, P. Cao, Predicting path-dependent diffusion barrier spectra in vast compositional space of multi-principal element alloys via convolutional neural networks, Acta Mater. 237 (2022) 118159.
- [17] J. Zhang, C. Wang, S. Huang, X. Xiang, Y. Xiong, B. Xu, S. Ma, H. Fu, J. Kai, X. Kang, S. Zhao, Design high-entropy electrocatalyst via interpretable deep graph attention learning, Joule 7 (2023) P1832–P1851.
- [18] S. Zhao, B. Jiang, K. Song, X. Liu, W. Wang, D. Si, et al., Machine learning assisted design of high-entropy alloys with ultra-high microhardness and unexpected low density, Mater. Des. 238 (2024) 112634, https://doi.org/10.1016/j. protect.2024.112634
- [19] J. Rickman, G. Balasubramanian, C. Marvel, H. Chan, M. Burton, Machine learning strategies for high-entropy alloys, J. Appl. Phys. 128 (2020) 221101.
- [20] R. Machaka, Machine learning-based prediction of phases in high-entropy alloys, Comput. Mater. Sci. 188 (2021) 110244.
- [21] R. Bobbili, B. Ramakrishna, V. Madhu, Development of machine learning based models for design of high entropy alloys, Mater. Technol. 37 (2022) 2580–2587.
- [22] L. Wu, T. Li, A machine learning interatomic potential for high entropy alloys, J. Mech. Phys. Solids 187 (2024) 105639.
- [23] I.A. Balyakin, A.A. Yuryev, B.R. Gelchinski, A.A. Rampel, Ab initio molecular dynamics and high-dimensional neural network potential study of VZrNbHfTa melt, J. Phys. 32 (2020) 214006.
- [24] J. Byggmästar, K. Nordlund, F. Djurabekova, Modeling refractory high-entropy alloys with efficient machine-learned interatomic potentials: defects and segregation, Phys. Rev. B 104 (2021) 104101.
- [25] J. Zhang, X. Liu, S. Bi, J. Yin, G. Zhang, M. Eisenbach, Robust data-driven approach for predicting the configurational energy of high entropy alloys, Mater. Des. 104 (2021) 104101.
- [26] X. Liu, J. Zhang, J. Yin, S. Bi, M. Eisenbach, Y. Wang, Monte Carlo simulation of order-disorder transition in refractory high entropy alloys: a data-driven approach, Comput. Mater. Sci. 187 (2021) 110135.
- [27] Y. Liu, T. Zhao, W. Ju, S. Shi, Materials discovery and design using machine learning, J. Materiomics 3 (2017) 159–177.
- [28] P. Ren, Y. Xiao, X. Chang, P.-Y. Huang, Z. Li, B.B. Gupta, X. Chen, X. Wang, A survey of deep active learning, ACM Comput. Surv 54 (2021) 1–40.
- [29] J.S. Smith, B. Nebgen, N. Lubbers, O. Isayev, A.E. Roitberg, Less is more: sampling chemical space with active learning, J. Chem. Phys. 148 (2018) 241733.
- [30] T.A. Young, T. Johnston-Wood, H. Zhang, F. Duarte, Reaction dynamics of diels-alder reactions from machine learned potentials, Phys. Chem. Chem. Phys. 24 (2022) 20820–20827.
- [31] G. Sivaraman, A.N. Krishnamoorthy, M. Baur, C. Holm, M. Stan, G. Csányi, C. Benmore, Á. Vázquez-Mayagoitia, Machine-learned interatomic potentials by active learning: amorphous and liquid hafnium dioxide, Npj Comput. Mater. 6 (2020) 104
- [32] S. Zhang, M.Z. Makoś, R.B. Jadrich, E. Kraka, K. Barros, B.T. Nebgen, S. Tretiak, O. Isayev, N. Lubbers, R.A. Messerly, J.S. Smith, Exploring the frontiers of condensed-phase chemistry with a general reactive machine learning potential, Nat. Chem. 16 (2024) 727–734.
- [33] J.S. Smith, B. Nebgen, N. Mathew, J. Chen, N. Lubbers, L. Burakovsky, S. Tretiak, H.A. Nam, T. Germann, S. Fensin, K. Barros, Automated discovery of a robust interatomic potential for aluminum, Nat. Commun. 12 (2021) 1257.
- [34] P. Yoo, M. Sakano, S. Desai, M.M. Islam, P. Liao, A. Strachan, Neural network reactive force field for C, H, N, and O Systems, Npj Comput. Mater. 7 (2021) 9.
- [35] V. Zaverkin, D. Holzmüller, I. Steinwart, J. Kästner, Exploring chemical and conformational spaces by batch mode deep active learning, Digit. Discov. 1 (2022) 605–620.
- [36] T. Young, T. Johnston-Wood, V. Deringer, F. Duarte, A transferable active-learning strategy for reactive molecular force fields, Chem. Sci. 12 (2021) 10944–10955.
- [37] S.J. Ang, W. Wang, D. Schwalbe-Koda, S. Axelrod, R. Gomez-Bombarelli, Active learning accelerates ab initio molecular dynamics on pericyclic reactive energy surfaces, Chem 7 (2020) 738–751.
- [38] T. Lookman, P.V. Balachandran, D. Xue, R. Yuan, Active learning in materials science with emphasis on adaptive sampling using uncertainties for targeted design, Npj Comput. Mater. 5 (2019) 1–17.
- [39] R. Xin, E.M. Siriwardane, Y. Song, Y. Zhao, S.-Y. Louis, A. Nasiri, J. Hu, Active-learning-based generative design for the discovery of wide-band-gap materials, J. Phys. Chem. C. 125 (2021) 16118–16128.
- [40] Z.W. Ulissi, A.J. Medford, T. Bligaard, J.K. Nørskov, To address surface reaction network complexity using scaling relations machine learning and DFT calculations, Nat. Commun. 8 (2017) 14621.
- [41] A. Seko, T. Maekawa, K. Tsuda, I. Tanaka, Machine learning with systematic density-functional theory calculations: application to melting temperatures of single- and binary-component solids, Phys. Rev. B. 89 (2014) 054303.
- [42] D. Khatamsaz, B. Vela, P. Singh, D.D. Johnson, D. Allaire, R. Arróyave, Bayesian optimization with active learning of design constraints using an entropy-based approach, Npj Comput. Mater. 9 (2023) 49.
- [43] D. Khatamsaz, B. Vela, P. Singh, D.D. Johnson, D. Allaire, R. Arróyave, Multiobjective materials bayesian optimization with active learning of design

- constraints: design of ductile refractory multi-principal-element alloys, Acta Mater. 236 (2022) 118133.
- [44] H. Zhang, H. Fu, Y. Shen, J. Xie, Rapid design of secondary deformation-aging parameters for ultra-low co content Cu-Ni-Co-Si-X alloy via Bayesian optimization machine learning, Int. J. Min. Met. Mater. 29 (2022) 1197–1205.
- [45] C. Chen, H. Zhou, W. Long, G. Wang, J. Ren, Phase prediction for high-entropy alloys using generative adversarial network and active learning based on small datasets, Sci. China Technol. Sci. 66 (2023) 3615–3627.
- [46] Z. Rao, P.-Y. Tung, R. Xie, Y. Wei, H. Zhang, A. Ferrari, T.P.C. Klaver, F. Körmann, P.T. Sukumar, A.K. da Silva, Y. Chen, Z. Li, D. Ponge, J. Neugebauer, O. Gutfleisch, S. Bauer, D. Raabe, Machine learning-enabled high-entropy alloy discovery, Science 378 (2022) 78–85.
- [47] D. Xue, P.V. Balachandran, J. Hogden, J. Theiler, D. Xue, T. Lookman, Accelerated search for materials with targeted properties by adaptive design, Nat. Comm. 7 (2016) 11241.
- [48] H. Li, R. Yuan, H. Liang, W.Y. Wang, J. Li, J. Wang, Towards high entropy alloy with enhanced strength and ductility using domain knowledge constrained active learning, Mater. Des. 223 (2022) 111186.
- [49] G.A. Sulley, J. Raush, M.M. Montemore, J. Hamm, Accelerating high-entropy alloy discovery: efficient exploration via active learning, Scr. Mater. 249 (2024) 116180.
- [50] Y. Zhang, C. Wen, C. Wang, S. Antonov, D. Xue, Y. Bai, Y. Su, Phase prediction in high entropy alloys with a rational selection of materials descriptors and machine learning models, Acta Mater. 185 (2020) 528–539.
- [51] J. von der Heyde, W. Malone, N. Zaman, A. Kara, Combining deep learning neural networks with genetic algorithms to map nanocluster configuration spaces with quantum accuracy at low computational cost, J. Chem. Inf. Model. 63 (2023) 5054–5055.
- [52] C. Henry, Catalytic activity of supported nanometer-sized metal clusters, Appl. Surf. Sci. 164 (2000) 252–259.
- [53] B. Johnson, Nanoparticles in catalysis, Top. Catal. 24 (2003) 147-159.
- [54] E. Tyo, Š. Vajda, Catalysis by clusters with precise numbers of atoms, Nat. nanotechnol. 10 (2015) 577–588.
- [55] Z. Michalewicz, C.Z. Janikow, Genetic algorithms for numerical optimization, Stat. Comput. 1 (1991) 75–91.
- [56] D.M. Deaven, K.M. Ho, Molecular geometry optimization with a genetic algorithm, Phys. Rev. Lett. 75 (1995) 288–291.
- [57] M.L. Paleico, J. Behler, Global optimization of copper clusters at the Zno(101⁻0) surface using a DFT-based neural network potential and genetic algorithms, J. Chem. Phys. 153 (2020) 054704.
- [58] E.L. Kolsbjerg, A.A. Peterson, B. Hammer, Neural-network-enhanced evolutionary algorithm applied to supported metal nanoparticles, Phys. Rev. B 97 (2018) 195424.
- [59] P.C. Jennings, S. Lysgaard, J.S. Hummelshøj, T. Vegge, T. Bligaard, Genetic algorithms for computational materials discovery accelerated by machine learning, npi Comput. Mater. 5 (2019) 46.
- [60] S. Heydariyan, M.R. Nouri, M. Alaei, Z. Allahyari, T.A. Niehaus, New candidates for the global minimum of medium-sized silicon clusters: a Hybrid DFTB/DFT genetic algorithm applied to Si_n , n=8-80, J. Chem. Phys. 149 (2018) 074313.
- [61] S. Darby, T.V. Mortimer-Jones, R.L. Johnston, C. Roberts, Theoretical study of Cu–Au nanoalloy clusters using a genetic algorithm, J. Chem. Phys. 116 (2002) 1536–1550.
- [62] R. Kelting, R. Otterstätter, P. Weis, N. Drebov, R. Ahlrichs, M.M. Kappes, Structures and energetics of small lead cluster ions, J. Chem. Phys. 134 (2011) 024311.
 [63] R. Kelting, A. Baldes, U. Schwarz, T. Rapps, D. Schooss, P. Weis, C. Neiss,
- F. Weigend, M.M. Kappes, Structures of small bismuth cluster cations, J. Chem. Phys. 136 (2012) 154309.
- [64] J.M. Jia, G.B. Chen, D.N. Shi, B.L. Wang, Structural and electronic properties of Bi_n (N=2-14) clusters from density-functional calculations, Eur. Phys. J. D 47 (2008) 359–365.
- [65] C. Seifried, L. Longo, P. Pollak, F. Weigend, The chemical space of $Pb_{N-n}Bi_n$ and $(Pb_{N-n}\,Bi_n)^+$: a systematic study for n=3-13, J. Chem. Phys. 146 (2017) 034304.
- [66] A. Larsen, J. Mortensen, J. Blomqvist, I. Castelli, R. Christensen, M. Dulak, J. Friis, M. Groves, B. Hammer, C. Hargus, E. Hermes, P. Jennings, P. Jensen, J. Kermode, J. Kitchin, E. Kolsbjerg, J. Kubal, K. Kaasbjerg, S. Lysgaard, J. Maronsson, T. Maxson, T. Olsen, L. Pastewka, A. Peterson, C. Rostgaard, J. Schiøtz, O. Schütt, M. Strange, K. Thygesen, T. Vegge, L. Vilhelmsen, M. Walter, Z. Zeng, K. Jacobsen, The atomic simulation environment a Python library for working with atoms, J. Phys.: Condens. Matter 29 (2017) 273002.
- [67] G. Kresse, J. Hafner, Ab initio molecular dynamics for liquid metals, Phys. Rev. B 47 (1993) 558, ibid. 49, 14 251 (1994).
- [68] G. Kresse, J. Furthmüller, Efficiency of ab-initio total energy calculations for metals and semiconductors using a plane-wave basis set, Comput. Mat. Sci. 6 (1996) 15–50.
- [69] G. Kresse, J. Furthmüller, Efficient iterative schemes for ab initio total-energy calculations using a plane-wave basis set, Phys. Rev. B 54 (1996) 11169.
- [70] J.P. Perdew, K. Burke, M. Ernzerhof, Generalized gradient approximation made simple, Phys. Rev. Lett. 77 (1996) 3865–3868.
- [71] P.E. Blöchl, Projector augmented-wave method, Phys. Rev. B. 50 (1994) 17953–17979.
- [72] K. Schütt, H. Sauceda, P. Kindermans, A. Tkatchenko, K. Müller, SchNet a deep learning architecture for molecules and materials, J. Chem. Phys. 148 (2017) 241722.